

# Free-edge Stress Singularities and Edge Modifications for Fiber Pushout Experiments

L. ROY XU,\* HUACHENG KUAI AND SREEPARNA SENGUPTA

*Department of Civil and Environmental Engineering &  
Interdisciplinary Materials Science Program  
Vanderbilt University  
Nashville, TN 37235, USA*

(Received February 14, 2004)

(Accepted August 30, 2004)

**ABSTRACT:** A comprehensive investigation of the fiber pushout test reveals that the existence of free-edge stress singularities hinder the accurate measurement of interfacial shear strengths. An integrated analytical, numerical, and experimental investigation is conducted to remove the free-edge stress singularities by modifying the edge design in a model fiber pushout test. The proposed interfacial joint angles are applicable to most composite material systems. The microdroplet test is recommended over the fiber pushout test since the convex shape of the microdroplet matrix makes it a natural choice.

**KEY WORDS:** adhesion, fiber pushout, interfacial strength, stress singularity, microdroplet test.

## INTRODUCTION

**D**ISSIMILAR MATERIAL INTERFACES/JOINTS can be found in numerous modern engineering and science fields. One major research effort in interface studies has been the evaluation of the interfacial strength of dissimilar materials [1–6]. Numerous studies have shown that failure often occurs along the interface/joint between two materials with high property mismatch (e.g., free-edge delamination in composite laminates and debonding between thin film/substrate), and that improving the interfacial properties (especially reducing the interfacial stress level) can modify the overall material/structural behavior [7–13]. Recent efforts also reveal that the chemical and mechanical aspects of interfacial bonding are essential for the nanostructured material development [14]. In fact, the interfacial bonding between the nanoscale reinforcement and the matrix

---

\*Author to whom correspondence should be addressed. E-mail: l.roy.xu@vanderbilt.edu

is the most important subject in the development of nanofiber composite materials [15]. For example, covalent binding is essential for the polymeric matrix nanocomposite material development. However, one important question is: can we evaluate the interfacial shear strength of nanofibers and the matrix using fiber pushout or pullout to examine the quality of covalent binding?

Since the interface plays an important role in the mechanical properties of fiber-reinforced composites, the role of the fiber–matrix interface in composite materials has been the focus of numerous investigations [7,16–28]. Single-fiber pullout and pushout tests, indentation techniques [29], microdroplet tests, and fragmentation tests are often employed to characterize the mechanical properties of the fiber–matrix interface. For example, Greszczuk [30] reported an early work conducted on the interface behavior using pullout and push-in tests. However, wide variations exist in experimental techniques, specimen processing, and assumptions used in constructing the models employed to derive interface properties from the above-named experiments. Consensus on the qualitative behavior and quantitative property estimates for interface properties [31,32] is often elusive due to the apparent scatter in the experimental data obtained from simplified mechanics models. Most difficulties in modeling arise from dealing with the conditions of adhesion, friction, and growth in debonding at the fiber–matrix interface [33]. Pitkethly et al. [34] reported a round-robin program carried out by 12 laboratories to assess the comparability amongst these various test methods, but the experimental results of interfacial shear strength differ depending on the particular laboratory and the test method. Therefore, explanations for the discrepancy and a reevaluation of the existing test methods for interfacial shear strengths were conducted extensively.

Originally, the interfacial shear strength tests were simply designed to ensure that the interface was mainly subjected to shear load. However, it is very important to examine the stress state at the interface ends since the theoretical linear elastic stress might be infinite at the free-edge (free-edge stress singularity). Beckert and Lauke [35] noticed that one of the most apparent problems of the single-fiber pullout test was the inhomogeneous interface stress state as a consequence of the geometrical discontinuities (fiber entry and fiber end point) acting as stress-concentrating elements. Ji et al. [36] introduced a method based on the singularity theory to discuss the micromechanics test specimen. It was concluded that the discrepancy amongst the different experiments arose from the stress singularity near the interface end. This was reconfirmed by Zheng and Ji [37], who employed the methods of asymptotic expansion and separation of variables to study the stress singularity near the interface ends of the specimens in push-in, pullout, and microdroplet tests. The existence of stress singularity at the interface ends hinders the accurate evaluation of interfacial shear strengths. This conclusion motivates us to investigate the existing test methods and, furthermore, to develop a more suitable test for interfacial shear strength evaluation.

From the above review, it is apparent that the macroscale interfacial strength measurement is still a major challenge due to the stress singularity problem [38,39]. Simultaneously, modern numerical tools such as the cohesive element method have an urgent need for interfacial strength and toughness values as important data input [40]. Hence, it is necessary to develop reliable, quantitative measurements in order to characterize the interfacial properties. Recently, Tandon et al. [41] proposed a novel cruciform specimen design to measure the interfacial tensile strength of fiber–matrix bonding, which was effective in reducing the free-edge effects. The key issue in measuring

intrinsic interfacial strengths is the creation of a uniform interfacial stress state. Hence, the first important step is the elimination of stress singularities. The objective of this investigation is to propose a new interfacial joint design for removing the stress singularity, which yields reasonable interfacial strength measurement for fiber pushout or pullout tests. In order to highlight the free-edge stress singularity and its modification, a model fiber pushout specimen, rather than an actual fiber pushout test (which is not convenient for *in situ* stress visualization), was employed to reveal the mechanics nature through an integrated numerical and experimental investigation. Similar model experiments were often employed [6,42,43], since the direct stress measurement around the actual fiber scales is still quite difficult and not easy for stress visualization. It should be noticed that under the same continuum interface mechanics scope, the scaling issue between the model fiber pushout tests and the actual fiber pushout test is not a concern for stress or failure visualizations. However, the size effect should be given enough attention if the failure strength values from the model fiber pushout test and the actual fiber pushout test were compared.

## THEORETICAL BACKGROUND

### Free-edge Stress Singularities in Dissimilar Material Interfaces/Joints

As illustrated in Figure 1(a), an Iosipescu shear test [44] was used to determine the interfacial shear strength of steel 4340 and Plexiglas (PMMA) joints [45]. Significant stress concentrations (caused by the free-edge stress singularity) were found at the bimaterial corners using the Coherent Gradient Sensing (CGS) technique, which was developed by Tippur et al. [46] for full-field mechanical–optical measurements. The CGS fringe patterns correspond to the gradients of  $\sigma_{xx} + \sigma_{yy}$ . It is this concentration/singularity that leads to a nonuniform interfacial stress distribution. It needs to be clarified here that

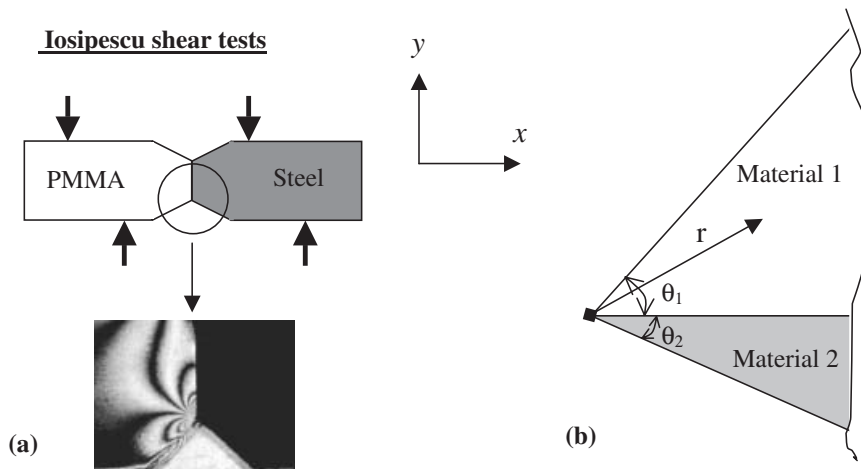


**Figure 1.** (a) Coherent Gradient Sensing (CGS) photograph showing a strong stress concentration (associated with fringe pattern concentrations) at the free edges of a bonded metal and polymer joint subjected to shear load [45] and (b) Angular definition of a bimaterial wedge.

the stress singularity is a mathematical phenomenon encountered in elastic stress solutions (infinite). On the other hand, the stress concentration is a physical phenomenon and refers to stress amplifications (finite), which is induced by the stress singularity in this investigation.

The existence of stress singularities for some specific bimaterial corners or edges was shown by Williams [47], Bogy [48], Hein and Erdogan [49], Genestedt and Hallstrom [50], Klingbeil and Beuth [51], Labossiere et al. [52], to name a few. The asymptotic stress field of a bimaterial corner can be expressed by:

$$\sigma_{ij}(r, \theta) = \sum_{k=0}^N r^{-\lambda_k} K_k f_{ijk}(\theta) \quad (i, j = 1, 2, 3) \quad (1)$$

where,  $f_{ijk}(\theta)$  is an angular function and  $K_k$  is also known as the ‘stress intensity factor.’ Although the fracture mechanics terminology ‘stress intensity factor’ is used in interfacial mechanics to characterize a similar stress singularity problem, it should be noticed that for an interfacial fracture problem (assuming initial debonding), the stress singularity at a crack tip is intrinsic and cannot be removed. However, the stress singularity in interfacial strength investigation (assuming perfect bonding) can be removed through an appropriate material design; a key issue in this investigation. The stress singularity order  $\lambda$  can be a complex number. Hence, the theoretical stress values will become infinite as  $r$  (defined in Figure 1(b)) approaches zero, if  $\lambda$  has a positive real part. This leads to a problem referred to as the ‘stress singularity problem.’ It is the presence of this stress singularity that leads to erroneous results in current interfacial strength measurements [38,41], besides being responsible for the free-edge debonding or delamination in dissimilar material joints. However, if  $\lambda$  has a nonpositive real part, then, the stress singularity disappears. Our major effort is focused on producing a nonpositive real part for  $\lambda$ , using an interfacial design approach.

Bogy [48] found that the stress singularity was purely determined by the material property mismatch and the two joint angles of the bimaterial corner  $\theta_1, \theta_2$  (defined in Figure 1(b)). Generally, the material property mismatch can be expressed in terms of the Dundurs’ parameters  $\alpha$  and  $\beta$  – two nondimensional parameters computed from four elastic constants of two bonded materials [53]:

$$\alpha = \frac{\mu_1 m_2 - \mu_2 m_1}{\mu_1 m_2 + \mu_2 m_1} \quad \beta = \frac{\mu_1(m_2 - 2) - \mu_2(m_1 - 2)}{\mu_1 m_2 + \mu_2 m_1} \quad (2)$$

where,  $\mu_1$  is the shear modulus of material 1,  $\mu_2$  is the shear modulus of material 2,  $\nu$  is the Poisson’s ratio,  $m = 4(1 - \nu)$  for plane strain, and  $m = 4/(1 + \nu)$  for generalized plane stress.

The stress singularity order is related to the material and geometric parameters, and is determined by a characteristic equation of coefficients  $A(\theta_1, \theta_2, p) - F(\theta_1, \theta_2, p)$ :

$$f(\theta_1, \theta_2, \alpha, \beta, p) = A\beta^2 + 2B\alpha\beta + C\alpha^2 + 2D\beta + 2E\alpha + F = 0 \quad (3)$$

where,  $p = 1 - \lambda$ .  $A$ ,  $B$ ,  $C$ ,  $D$ ,  $E$ , and  $F$  are expressed as follows [48]:

$$\begin{aligned}
 A(\theta_1, \theta_2, p) &= 4K(p, \theta_1)K(p, \theta_2), \\
 B(\theta_1, \theta_2, p) &= 2p^2 \sin^2(\theta_1)K(p, \theta_2) + 2p^2 \sin^2(\theta_2)K(p, \theta_1), \\
 C(\theta_1, \theta_2, p) &= 4p^2(p^2 - 1) \sin^2(\theta_1) \sin^2(\theta_2) + K[p, (\theta_1 - \theta_2)], \\
 D(\theta_1, \theta_2, p) &= 2p^2[\sin^2(\theta_1) \sin^2(p\theta_2) - \sin^2(\theta_2) \sin^2(p\theta_1)], \\
 E(\theta_1, \theta_2, p) &= -D(\theta_1, \theta_2, p) + K(p, \theta_2) - K(p, \theta_1), \\
 F(\theta_1, \theta_2, p) &= K[p, (\theta_1 + \theta_2)]
 \end{aligned} \tag{4}$$

where the auxiliary function  $K(p, x)$  is defined by:

$$K(p, x) = \sin^2(px) - p^2 \sin^2(x). \tag{5}$$

Our basic idea is to vary these four independent parameters  $(\theta_1, \theta_2, \alpha, \beta)$  in order to obtain a negative real value of the stress singularity order  $\lambda$ . In such a scenario, the stress distribution close to the free edge is not expected to be very sharp.

### Convex Interfacial Joints for Uniform Interfacial Stress Distribution

Indeed, nature has already provided us with a nice solution to reduce or eliminate the stress singularity at the bimaterial edge. Mattheck [54] analyzed an interesting problem of a tree–steel railing interface. His finite element analysis showed that for a total convex joining angle  $\theta_1 + \theta_2 = 270^\circ$ , the Mises stress has a concentrated value at the joint corner. The optimization of his problem proved that a convex joint would be a better design. The mechanics foundation of such a joint could be explained by Bogy's work. Since appropriate angular combinations  $(\theta_1, \theta_2)$  can be selected depending on different material combinations, it is possible to obtain a negative or zero value for  $\text{Re}(\lambda)$ . This means that the degree of singularity can be reduced or removed. We start from a simple example to illustrate the general principle.

The model interface used in this investigation was a polycarbonate (PC)–aluminum (Al) interface/joint. Generalized plane stress conditions were considered in computing the Dundurs' parameters,  $\alpha = -0.935$  and  $\beta = -0.308$ . According to our numerous case studies, if we choose an interfacial design with joint angles:  $\theta_1 = 45^\circ$  and  $\theta_2 = 65^\circ$ , and assumed material 1 to be a typical soft material and material 2 to be hard, then, no stress singularity exists for a wide range of engineering materials. This result is illustrated in Figure 2(a) for the entire possible range of the two Dundurs' parameters [8]. It can be seen that for this specific pair of joint angles, the stress singularity is limited to a very small zone near  $\alpha \cong 1$ . Such extreme material joint combinations are quite rare in engineering applications since they represent extremely high mismatch in the Young's moduli (Young's moduli relation:  $E_2 > E_1$ ). Recent examples include nanotube/nanofiber-reinforced polymer composites – the Young's modulus of carbon nanotubes is as high as 1000 GPa, while the Young's modulus of general polymer matrices is around 5 GPa [15]. Since the brittleness of the fiber resists machining, we proposed another combination of convex joint angles, as illustrated in Figure 2(b), which could be easily adopted by the tests at hand. Although this joint angle combination has a relatively larger singular zone than the one shown in Figure 2(a), it is still applicable since  $\alpha$  is less than 0.8 for most

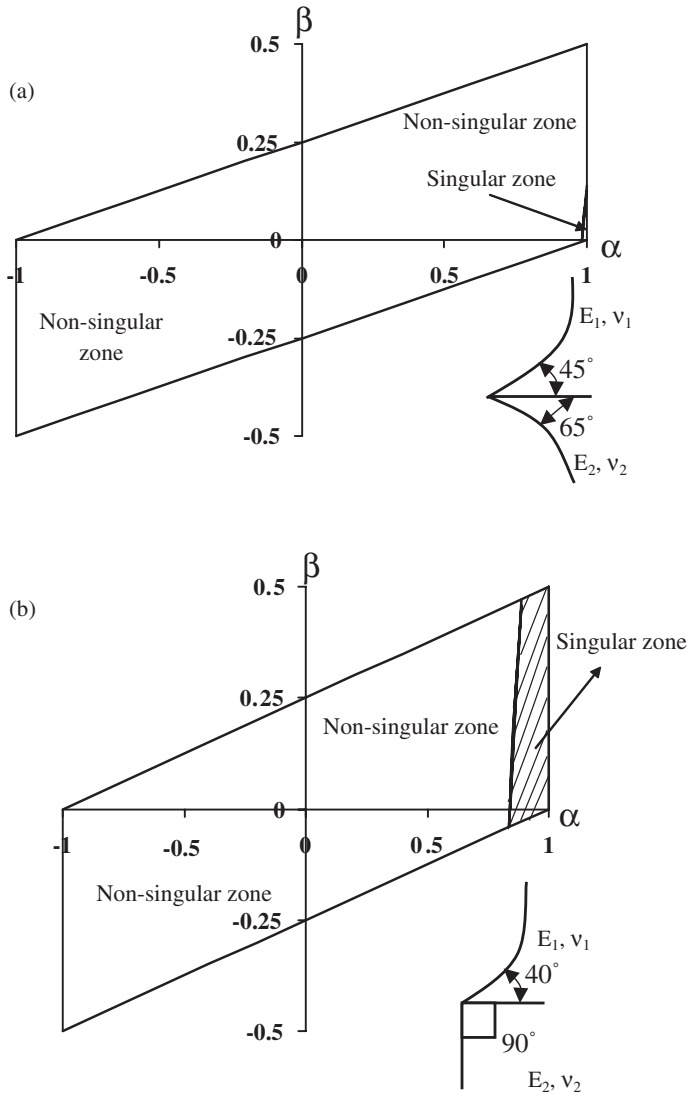


**Figure 2.** Stress singularity order  $\lambda$  as a function of two Dundurs' parameters for two proposed pairs of joint angles (materials 1 and 2 are soft and hard materials, respectively). A small singular zone implies the given pair of joint angles is applicable for a wide range of engineering material combinations.

composite systems [8]. The advantage of the proposed 90–40° angular combination will be further analyzed by the finite element method.

### SPECIMEN DESIGN AND NUMERICAL ANALYSIS

The purpose of numerical analysis is to provide guidance for the determination of specimen design parameters and to compare the stress fringe patterns with those obtained from experimental investigation.

**Finite Element Modeling**

The linear elastic finite element analysis of the proposed convex aluminum–polycarbonate fiber pushout specimen, under plane stress condition, was carried out, employing the commercial software ANSYS. In this investigation, two different interfacial joints, with the same material combination and bonding area, were subjected to the same pushout load and their results were compared, as shown in Figure 3. One was used to simulate the traditional pushout specimen with straight free-edges (Figure 3(a)). It was expected that severe stress singularity would be observed in this baseline specimen. The modified specimen had convex edges with proposed specific interfacial joint angles, as seen in Figure 3(b). The dimensions of the baseline specimen are shown in Figure 3. In order to obtain more *in situ* fringes during the loading process, the specimen thickness was adopted as 9.2 mm. In the finite element analysis, taking advantage of symmetry, only half of the specimen was modeled. For the edge-modified specimen, the transition from the straight-edge to the curved edge at the interface corner was achieved by means of a circular arc of radius  $R = \{t * \tan(45 + \theta/2) / \cos(\theta)\}$ , where  $\theta$  is the joining angle and  $t$  is the convex

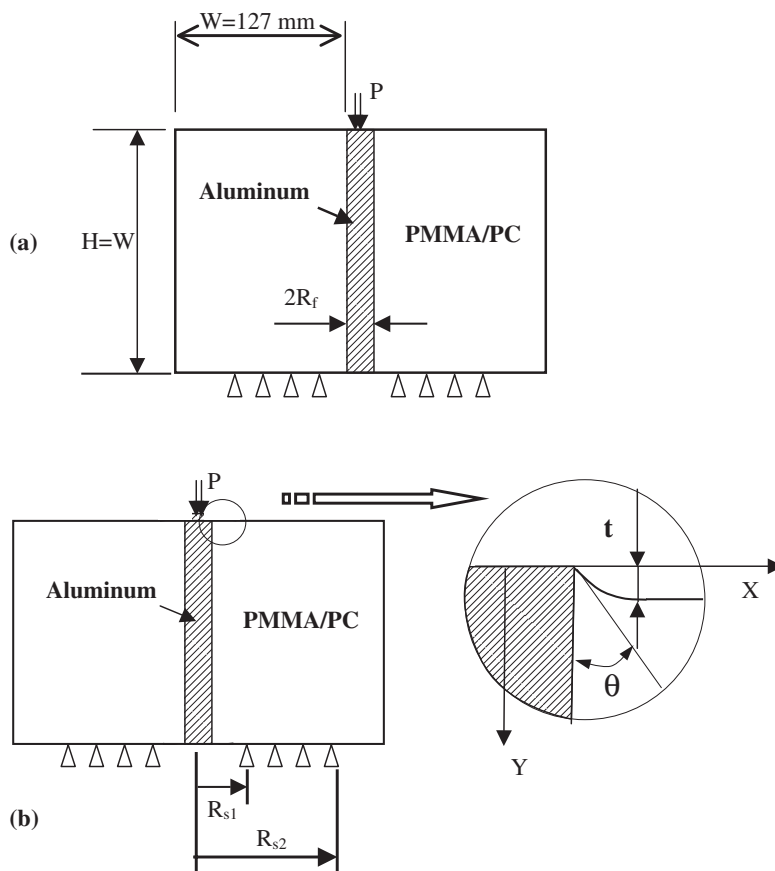


**Figure 3.** Plane-stress model fiber pushout specimens (a) baseline straightedged; (b) only matrix-shaped (width of the aluminum model fiber  $2R_f=9.1$  mm; distance of the support away from the center line  $R_{s1} = 16.5$  mm,  $R_{s2} = 63.5$  mm). Thickness of specimens = 9.2 mm.

extension distance as illustrated in Figure 3(b). Roller boundary conditions were applied along the midplane of the specimen, i.e., at  $x=0$ . Besides, supports were provided along the bottom edge of the specimen by specifying zero vertical displacement from distances  $R_{s1}$  to  $R_{s2}$ , the values of which are given in Figure 3. It may be noticed that in contrast to modeling of the actual fiber pushout test, contact elements were not used along the interface, since the focus of this investigation is to analyze the interfacial stress distribution before the interface crack initiation.

The finite element mesh consisted of PLANE 42 elements (2D four-noded elements) and  $h$ -version refined elements were employed in the regions where the stress gradient was expected to be high. A total of 23,090 elements were used in meshing the shaped matrix specimen of which 3671 elements were used in meshing the model aluminum fiber. The element length along the interface varied from a maximum of 0.33 mm ( $0.0026H$ ) to a minimum of 0.0013 mm, where  $H$  is the height of the specimen (127 mm). Maximum refinement, of course, was employed at the interface corner. The meshes used in the baseline and the modified specimens were almost similar. For the straightedged baseline specimens, the element length ranged from a maximum of  $0.1W$  to a minimum of  $0.000407W$ , where  $W$  is the specimen width (127 mm). While the maximum element edge length was retained in meshing the shaped specimens, the smallest element length was changed to  $0.000794W$  in order to utilize the same meshing pattern for both modified and baseline (straightedge) specimens. The model fiber (aluminum) and the model matrix (polycarbonate) were defined as linearly elastic and isotropic materials, and their stiffness properties for aluminum were chosen as  $E=71$  GPa,  $\nu=0.33$  and for polycarbonate,  $E=2.4$  GPa,  $\nu=0.34$ . The finite element simulations were run for different load levels ranging from  $P=1000$  to 4000 N to verify the reduction of the free-edge stress singularity. As such, the specimen was not loaded till failure and hence, no failure criterion was defined.

### Influence of Geometric Shapes

The main parameters that have been varied in our finite element analysis are (a) the convex extension distance  $t$  and (b) the interfacial joining angles. The influence of these geometrical parameters, on the stress distribution at the interface, has been illustrated in Figures 4 and 5. Four cases have been examined viz.  $t=0$  (straightedge or baseline specimens), 1.0, 3.0, and 5.0 mm. For zero extension distance, i.e., straightedged specimens, a prominent sharp stress distribution is seen at the intersection of the bimaterial interface as shown in Figure 4. However, for increasing extension distances, the interfacial shear stress distributions are seen to smoothen out over the interface to uniform values. From this analysis, we find that the free-edge stress singularity is successfully removed and the convex extension distance  $t$  mainly affects local stress distributions close to the free-edges.

However, the proposed specimen dimensions may not be accurately machined. So a question naturally arises: should we use the exact  $90^\circ$ – $40^\circ$  combination only? Figure 5 is significant in that while only the  $90^\circ$  angle of the fiber material was retained and the joint angle of polycarbonate was varied from  $40^\circ$  to  $90^\circ$ , the stress singularity was effectively removed for the  $90^\circ$ – $40^\circ$  and  $90^\circ$ – $60^\circ$  combinations (as per Figure 5(b) and (c)). This essentially points to the fact that, a conclusive solution for the stress singularity reduction has been arrived at, as long as the sum of two joint angles is less than  $180^\circ$  and each joint angle is less than  $90^\circ$  [55].

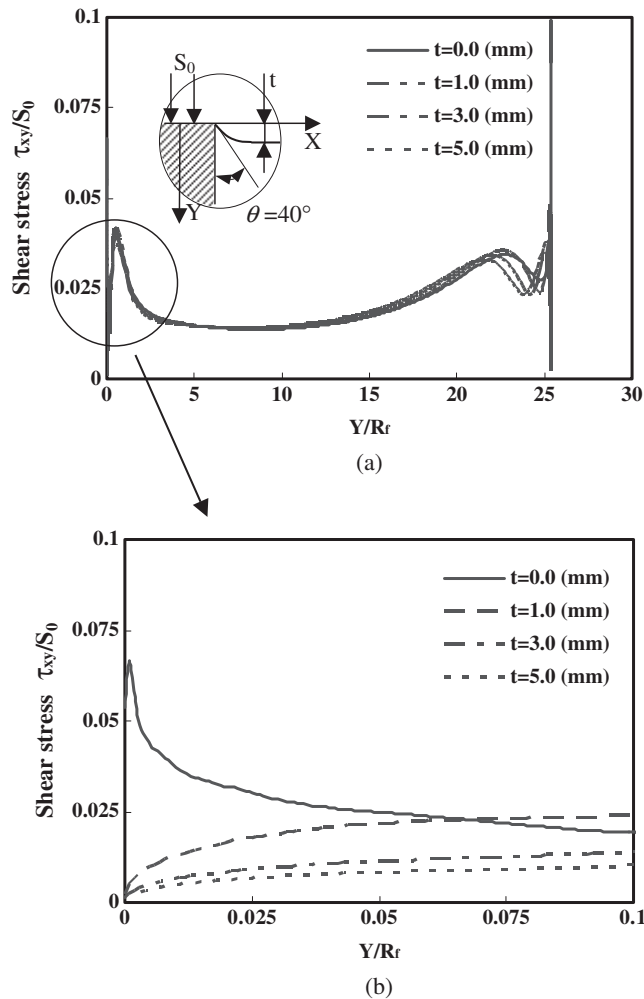


**Figure 4.** Finite element analysis: the influence of various extension distances on the normalized interfacial shear stress distribution with two fixed joint angles (a) along the whole interface and (b) around one end of the fiber (range of applied stress on the model fiber is 5.5 mm, less than the fiber width (9.1 mm)).

As mentioned before, the brittleness of the fiber does not afford machining and hence, the finite element analysis was used to determine whether both the fiber and the matrix needed to be given a convex shape or whether only a convex-shaped matrix would serve the purpose. Figure 6 illustrates the effectiveness of our simple modification. As seen in Figure 6(a), there was very little difference in global interfacial shear stress distributions for the three different types of interfacial edge combinations, i.e., (a) baseline straight-edge case, (b) only matrix-shaped case, and (c) both the fiber and the matrix-shaped case. Indeed, if the local stress states were examined as seen in Figure 6(b), the stress distribution difference between the two edge-modification cases (b) and (c) is small enough to be neglected. Both convex joint cases could successfully remove the free-edge stress singularity. Based on this numerical result and the inconvenience in machining of the fiber, only the matrix-shaped fiber pushout test is recommended in this investigation.

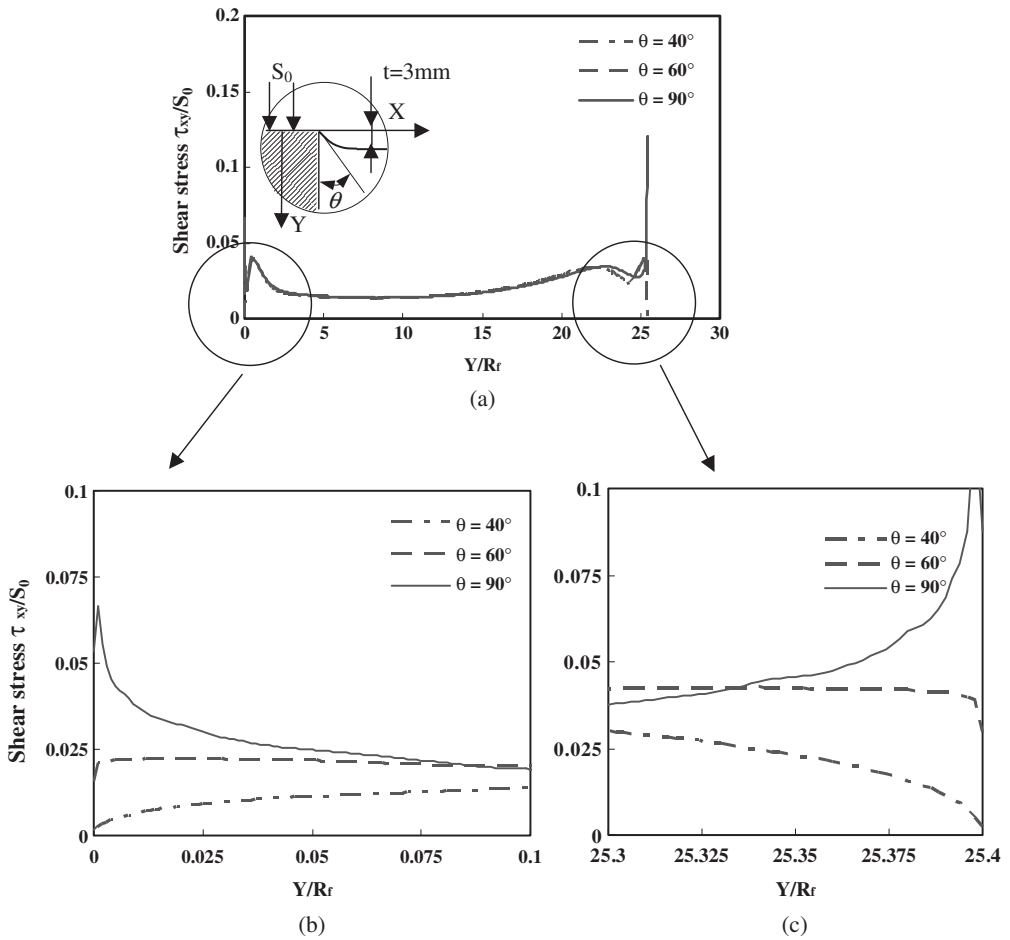


**Figure 5.** Finite element analysis: the influence of the matrix joint angle on the normalized interfacial shear stress distribution (a) along the whole interface (b) and (c) around two ends of the model fiber (range of applied stress on the model fiber is 5.5 mm).

### EXPERIMENTAL INVESTIGATION

The major purpose of this experimental study is to verify that the new edge design is effective in removing the free-edge stress singularity for fiber pushout/pullout experiments. *In situ* photoelasticity experiments of plane polymer–metal specimens are employed.

#### Specimen Preparation

Two types of specimens were designed and prepared for comparison, as seen in Figure 3. The straightedge specimen was treated as the baseline for comparison and our focus was on the modified pushout specimen as illustrated in Figure 3(b). For all the specimens, the test materials used were polycarbonate, to simulate the matrix material and aluminum

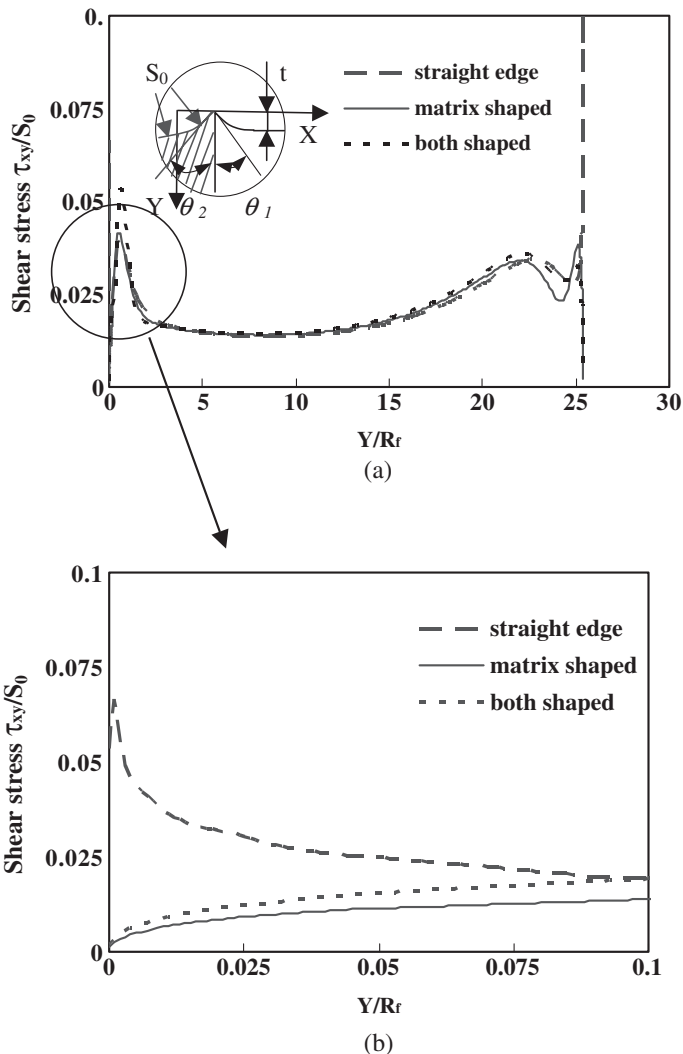


**Figure 6.** Finite element analysis: the influence of the interfacial joint angles on the normalized interfacial shear stress distribution (a) along the whole interface and (b) around one end of the model fiber (Extension distance  $t=3$  mm, matrix joint angle  $\theta_1=40^\circ$  for the shaped model matrix, fiber joint angle  $\theta_2=60^\circ$  for the shaped model fiber).

to simulate the fiber material. Weld-on-10 adhesive (Meyer Plastics, Inc.) was used as the bonding agent since its properties are close to those of PMMA or polycarbonate [46]. Thereby, the possible involvement of a third material in a typical bimaterial problem was eliminated. The adhesive had two components, A and B. They were mixed before bonding and cured at room temperature for at least 4 h. After 24 or 48 h, the adhesive bonding reached the design strength. Before bonding, the bonding areas were sand blasted and cleaned. A special fixture was designed to bond these specimens. The alignment of these specimens was carefully examined during the bonding process.

### Experimental Setup

A mechanical–optical system was used to record the *in situ* fringe pattern development during the loading process, as shown in Figure 7. The entire setup consisted of an optical system, a mechanical testing system, and an imaging system. The mechanical testing system included an MTS 810 test machine. The optical system was utilized to capture the *in situ* fringe pattern development (related to in-plane stress development) during the tests. A laser beam was transmitted through the transparent polymeric specimen, and the resulting fringe pattern was recorded by a camera. Photoelasticity experiments were performed for the polycarbonate specimens. The isochromatic fringe patterns observed were the contours of the maximum in-plane shear stress,

$$\tau_{\max} = (\sigma_1 - \sigma_2)/2 = \frac{Nf_{\sigma}}{2h} \quad (6)$$

where,  $\sigma_1$  and  $\sigma_2$  are in-plane principal stresses,  $N$  is the fringe order,  $f_{\sigma}$  is the stress-fringe constant and  $h$  is the specimen thickness (Kobayashi, 1987).

The optical system included a He–Ne laser source (17 mW), a laser collimator, a reflection mirror, and two circular polarizer sheets for photoelasticity experiments. The function of the collimator was to provide a large and collimated laser beam (diameter 50 mm) since the field of view of our specimens was at least 10 mm. The purpose of the mirror was to adjust the laser beam to a desired position for a specific experiment. The imaging system included a high-resolution digital camera to capture the fringe development and a density filter in front of the camera to reduce the laser intensity, since the laser beam entered the camera directly. Because the laser beam diameter was approximately 50 mm, a convex lens (focal length 150 mm) was added to the system to record the full image. An important issue in obtaining good-quality photos is that the digital camera should be focused at infinity, and that the distance between the convex lens and the

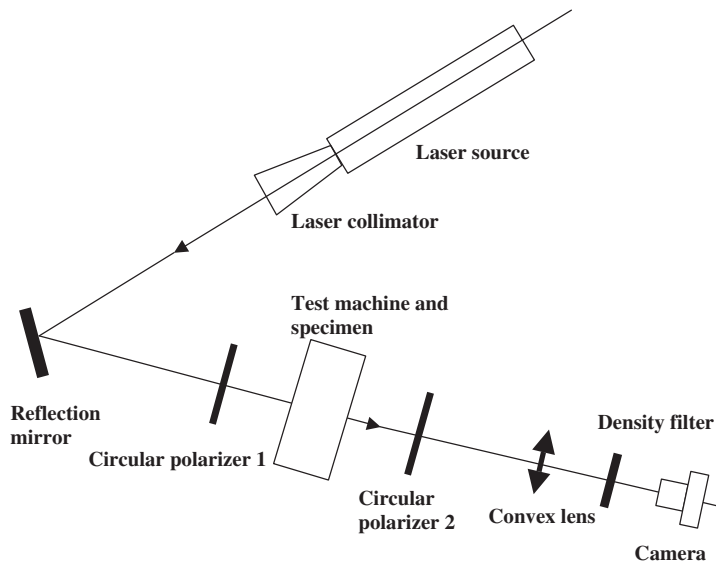


**Figure 7.** Experimental setup of a mechanical–optical system to record *in situ* stress development during loading process.

specimen should be slightly larger than the focal length of the convex lens. Each specimen was loaded to a certain level such as 1kN, 2kN, and then *in situ* fringe patterns were recorded. The specimen was not loaded to failure since our major focus was to examine the elimination of the free-edge stress singularity in the model fiber pushout experiments.

## RESULTS AND DISCUSSIONS

### Comparison of Numerical Analysis with Experimental Results

Full-field photoelasticity results can be employed to make a direct comparison with the finite element simulation. In order to calibrate the stress-fringe constant of polycarbonate used in this investigation, an indentation experiment was conducted and the experimental fringe pattern was directly compared to the numerical pattern generated by finite element analysis, as shown in Figure 8. Figure 8(a) is a photoelasticity picture of a polycarbonate plate subjected to pushout load from an indenter as illustrated in Figure 8(c). Figure 8(b) shows the corresponding fringe patterns under the same applied load 1000 N. After the fringe order  $N$  was computed at every node using Equation (6), a counterplot was

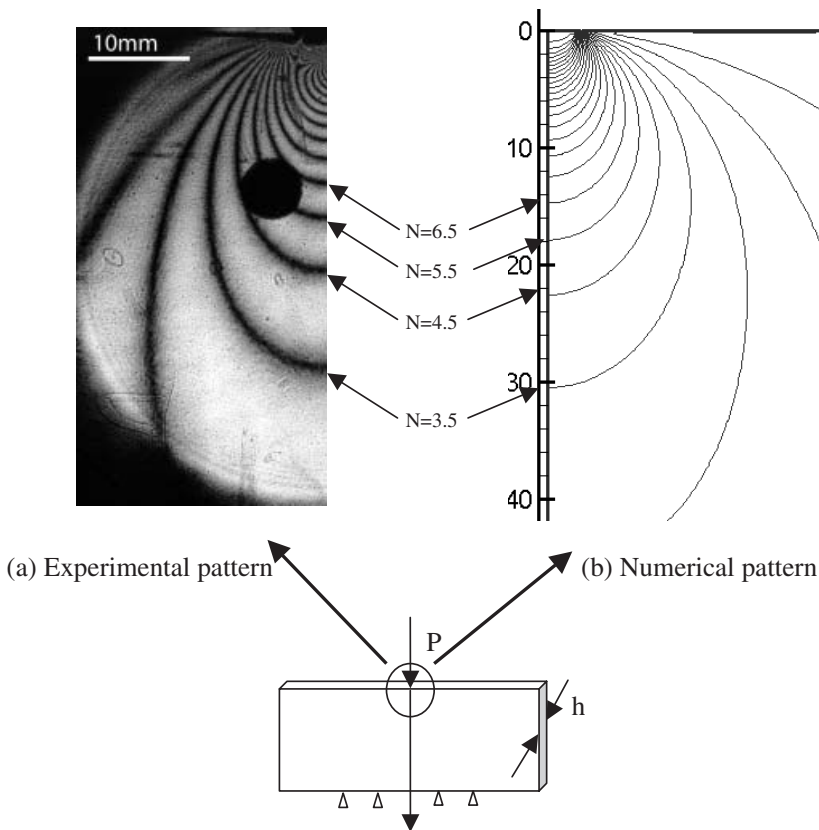


**Figure 8.** Comparison of the photoelasticity fringe patterns of a polycarbonate specimen subjected to pushout loading (a) experimental pattern and (b) numerical pattern for  $P = 1000\text{ N}$ . Low support is symmetric along the center line of the specimen; distances of the support away from the center line are 16.5–63.5 mm.

obtained for a numerical fringe pattern. Excellent agreement was obtained. Therefore, in other more complicated pushout experiments involving model fibers and matrices, more theoretical fringe patterns were generated for comparison with experimental investigation. After the fringe order  $N$  was computed at every node using Equation (6), a corresponding gray-scale value was calculated by associating a gray-scale value of 255 with full fringe orders (e.g., 0, 1, 2, etc) and a value of 0 with half fringe orders (e.g., 0.5, 1.5, 2.5, etc). The plotting software Tecplot 9.2 was then used to plot these gray-scale values, and the numerical fringe patterns shown in Figures 9 and 11 were generated for stress field visualization and comparison with experimental results.

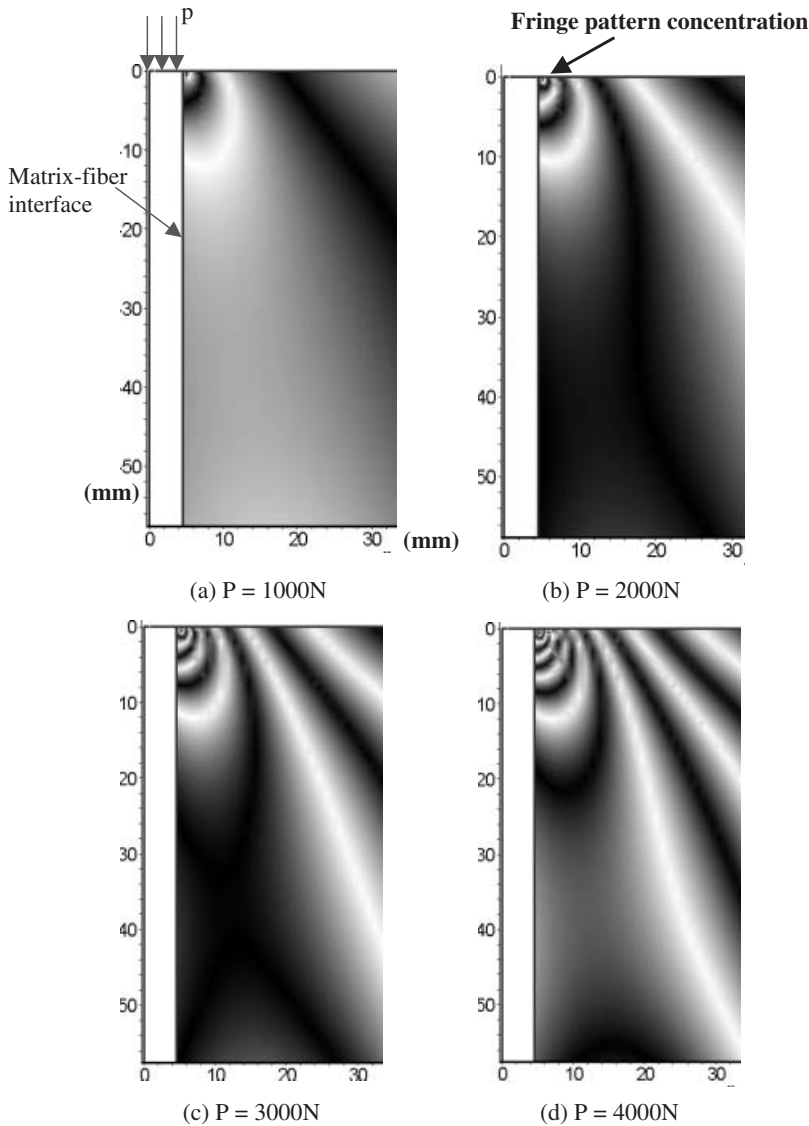


**Figure 9.** Numerical simulation of fringe pattern development in a straightedge specimen under different applied load levels.

It is rather interesting to note that a clear stress fringe concentration originates at the interface corner for straightedged specimens with increasing load, as shown in Figure 9. This type of fringe concentration is a result of free-edge stress singularity and is very similar to the fringe concentration caused by a bimaterial interfacial crack [56]. We notice that the stress singularity order for Al/PC joints is around  $-0.2$  and can be eliminated, but for interfacial cracks, the stress singularity order is  $-0.5 + i\epsilon$  [8,57] and is intrinsic. A direct comparison of the numerical fringe pattern (Figure 9(d)) and the experimental pattern (Figure 10(d)) of the same specimen subjected to the same applied load of 4000 N verifies the existence of stress singularity at the free edge. It should be noticed that the fringe

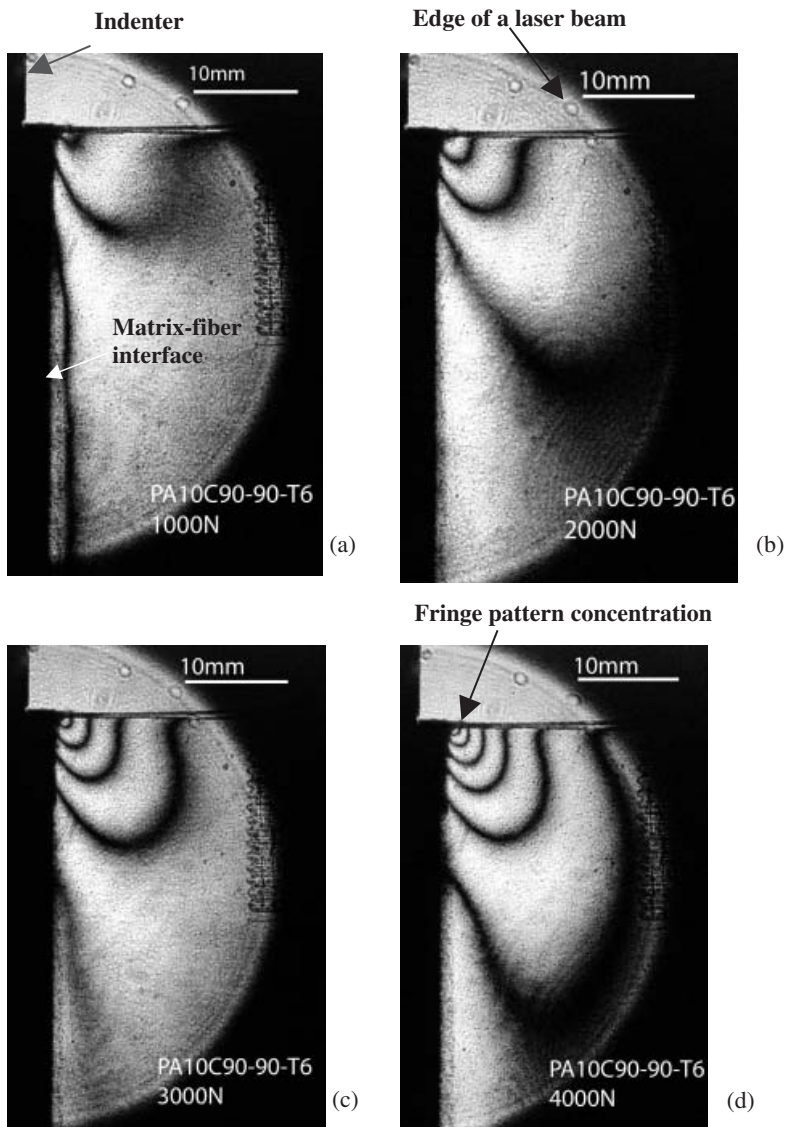
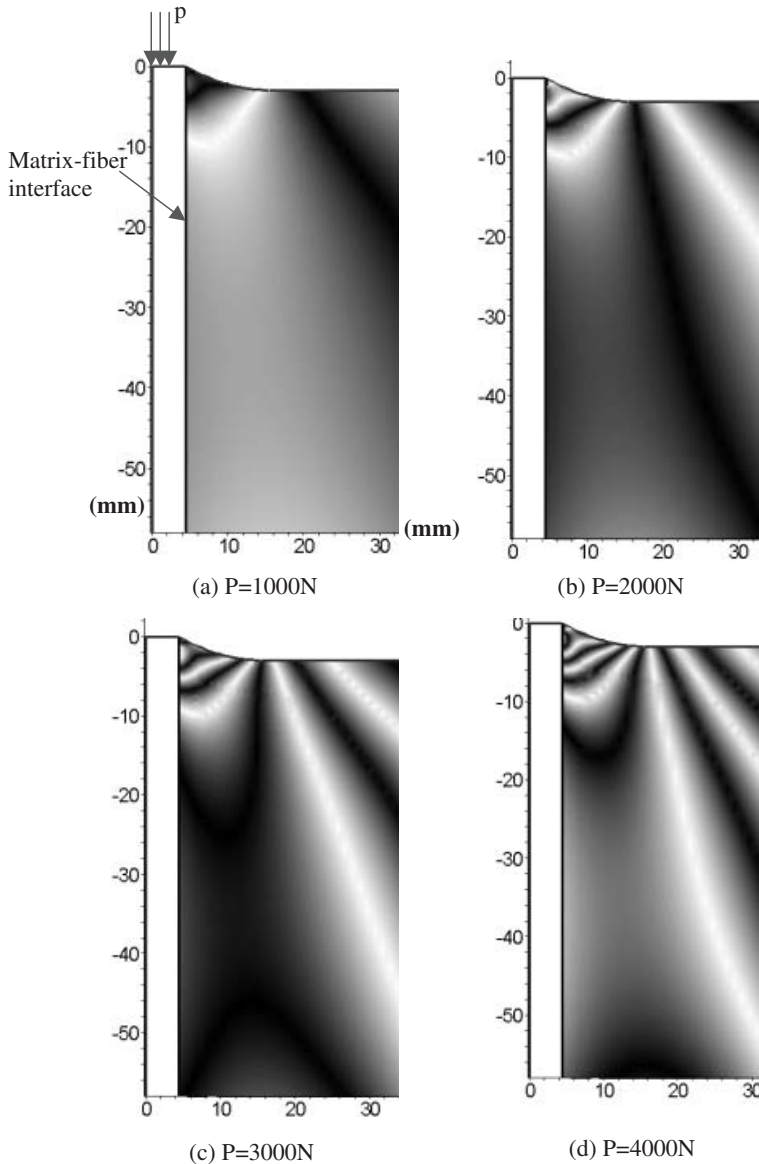
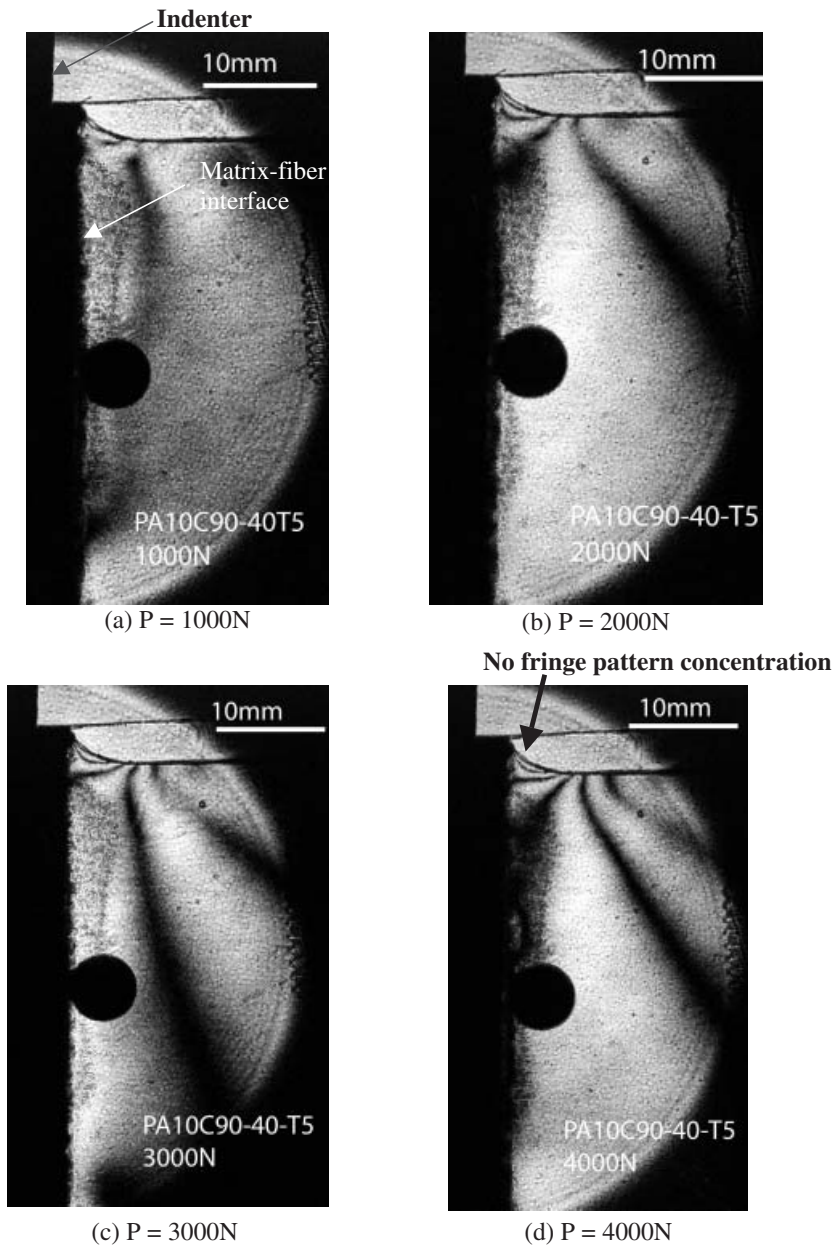


Figure 10. In situ pictures of fringe pattern development in a straightedged specimen under different applied load levels.

pattern concentration is not very clear for small applied load (e.g., 1000 N in Figure 9(a)). Similar results were reported by Bechel and Sottos [24] and Tandon et al. [41]. The accumulation of fringes at the bimaterial interfacial corner, seen in the straightedged specimens, completely disappeared in the photoelastic fringe patterns for the shaped specimen as seen in Figure 11. The experimental fringe pattern also validates this result as shown in Figure 12. This is a clear indication that the stress singularity has been removed in the proposed convex joint. Therefore, a more general question arises regarding the



**Figure 11.** Numerical simulation of fringe pattern development in an edge-modified specimen under different applied load levels.



**Figure 12.** In situ pictures of fringe pattern development in an edge-modified specimen under different applied load levels.

definition of the interfacial strength measurement for composite or dissimilar materials. It should be noted that our experimental observation and finite element analysis all showed that our specimens and the actual fiber pushout specimens failed in tension (not shear) from the lower interface, due to the bending effect of the lower support. So the measured data (failure force/interface area) were not actual interfacial shear strengths.

## Comparison of Traditional Strength and Interfacial Strength Measurements

The strength definition of a homogeneous material is quite straightforward: it is the failure stress of the specimen with a uniform stress state across the cross section. Since the final failure of the material is associated with the initial defect distribution at the cross section, specimens with different sizes will yield different strength data (e.g., Weibull strength distribution) although there is no length scale involved in the stress distribution of these specimens. This phenomenon may be defined as ‘the material size effect.’ As discussed before, the interfacial strength measurement is quite complicated because of the possible stress singularity and the highly nonuniform interfacial stress distributions as shown in Figure 4(b). Therefore, any interfacial strength experiment must be carefully examined, otherwise it may yield meaningless data.

For a specimen constituted of the same material, the size effect still exists due to initial material defects, although these types of specimen have no length-scale involved in terms of their stress states. However, for a specimen fabricated from two dissimilar materials (a typical example of current material test standards) shown in Figure 4(b), the shear stress distribution across the interface is not uniform according to previous theoretical analysis and experimental verification. The asymptotic stress field at the bimaterial corner is related to a significant length scale  $r^{-\lambda}$ . Obviously, this type of specimen will provide data with a strong size effect in the context of mechanical behavior. Moreover, the mechanics size effect (related to the stress singularity) will be coupled with the material size effect, and thus lead to complexities in measurement data, which cannot be treated as intrinsic material properties. Therefore, the measured nominal interfacial strengths based on current test standards cannot be used in mechanics predictions because the interfacial properties obtained from laboratory tests are quite different from the real values of structures in service. For example, two kinds of PMMA/Al bimaterial specimens, with the same interface area but different joint angles, should yield the same final failure load, if the interfacial strength is assumed to be indeed a material constant. However, our experimental results show that the difference of these two failure load values was up to 58% [55]. The influence of the stress state on the failure strength is further illustrated in Figure 13. Figure 13(b) is an Iosipescu shear specimen for the shear strength measurement for composite materials, and other materials. Figure 13(a) is its original beam counterpart without the V-notch modification subjected to the same applied load. It should be noticed that the transverse shear stress states of these two kinds of specimens are quite different. For the straightedge beam specimen in Figure 13(a), the shear stress distribution will be a parabolic distribution and is not uniform. So the final shear failure will generally not initiate from the upper and lower edges of the beam specimen due to a very low shear stress. On the other hand, a uniform shear stress distribution could be achieved in the Iosipescu shear specimen so the final shear failure might occur at any location. Indeed, the experimental results showed that the average shear strengths from these two specimens were quite different although the same material was used in these specimens [55].

Owing to the stress singularity at the free edge, failure of the bimaterial specimen always initiated at the specimen edge rather than at the center in all our earlier experiments [45]. Hence, the interfacial strength from the current measurement standard is directly related to the singular stress state and initial defects at the edge only, rather than to a uniform stress state and taking into account all initial material defects at the whole interface. In order to measure an intrinsic interfacial strength, a uniform stress distribution across the interface should be created. Thus, all initial defects will have an equal probability of

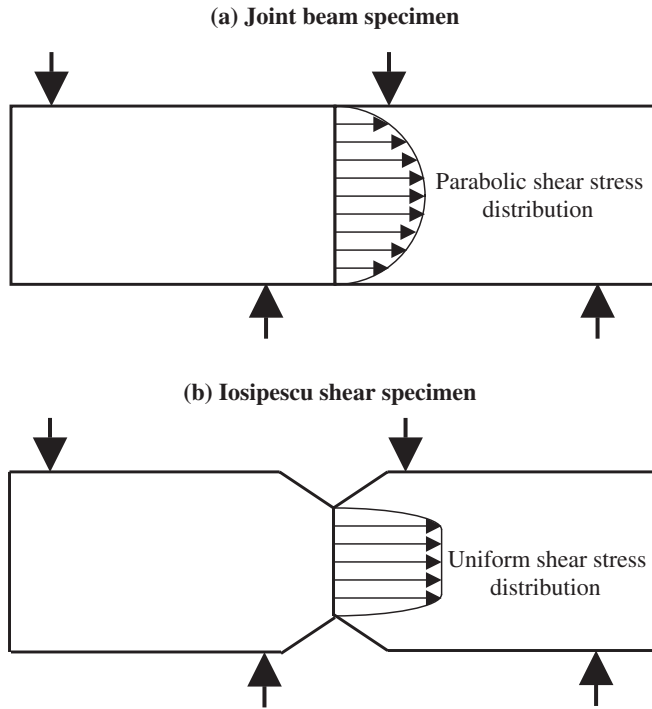


**Figure 13.** Interfacial shear stress distributions of (a) joint beam specimen – parabolic distribution and (b) Iosipescu shear specimen – uniform distribution.

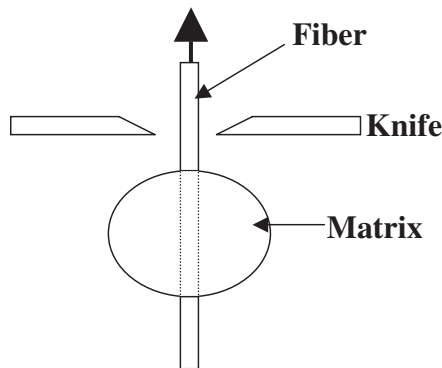


**Figure 14.** Schematic diagram of a microdroplet test.

leading to final failure (breaking the interface). This kind of strength data should be very close to intrinsic tensile strengths when the interface is loaded to failure. It is naturally expected that the current convex joint specimen should yield a reasonable interfacial strength value since the interfacial shear stress is quite uniform as seen in Figure 4. A possible problem is how to achieve the convex interfacial joint for a microscale fiber pushout specimen. It was then noticed that another interfacial shear strength test, the microdroplet test, just satisfied the requirement of our suggested convex interfacial joint. As seen in Figure 14, a matrix drop just forms a convex joint with the fiber. Free-edge

stress singularities, commonly seen in all kinds of fiber pushout or pullout tests, are thus not encountered in the microdroplet test. It is not surprising that the interfacial shear strength values measured from the traditional fiber pushout tests and the microdroplet tests are quite different. According to this investigation, interfacial shear strength values measured from the microdroplet test are more reasonable.

## CONCLUSIONS

It has been concluded that convex interfacial joints are quite effective in eliminating free-edge stress singularities in fiber pushout tests after an integrated analytical, numerical, and experimental investigation. The proposed interfacial joint angles are applicable to most composite material systems. The microdroplet test is recommended over the fiber pushout test since the convex shape of the microdroplet matrix makes it a natural choice.

## ACKNOWLEDGMENTS

L.R.X. gratefully acknowledges the support from the Office of Naval Research Young Investigator Award (N00014-03-1-0505), and the National Science Foundation, Surface Engineering and Materials Design Program (CMS-0409665).

## REFERENCES

1. Drzal, L.T. (1990). Fiber-matrix Interphase Structure and its Effect on Adhesion and Composite Mechanical Properties, In: Ishida, H. (ed.), *Controlling Interphases in Composite Materials*, pp. 309–319, Elsevier, Amsterdam.
2. Hsueh, C.H. (1990). Interfacial Debonding and Fiber Pull-out Stresses of Fiber-Reinforced Composites, II: Non-Constant Interfacial Bond Strength, *Materials Science and Engineering A*, **125**: 67–73.
3. Stanford, J.L., Lovell, P.A., Thongpin, C. and Young, R.J. (2000). Experimental Studies on the Interfacial Shear-transfer Mechanism in Discontinuous Glass-fiber Composites, *Composites Science and Technology*, **60**: 361–365.
4. Lin, G., Geubelle, P.H. and Sottos, N.R. (2001). Simulation of Fiber Debonding with Friction in a Model Composite Pushout Test, *International Journal of Solids and Structures*, **38**: 8547–8562.
5. Zhou, X.-F., Wagner, H.D. and Nutt, S.R. (2001). Interfacial Properties of Polymer Composites Measured by Push-out and Fragmentation Tests, *Composites Part A*, **32**: 1543–1551.
6. Li, Z., Bi, X., Lambros, J. and Geubelle, P.H. (2002). Dynamic Fiber Debonding and Frictional Pushout in Model Composite Systems: Experimental Observations, *Experimental Mechanics*, **42**: 417–425.
7. Kerans, R.J., Hay, R.S., Pagano, N.J. and Parthasarathy, T.A. (1989). The Role of the Fiber-Matrix Interface in Ceramic Composites, *Ceramic Bulletin*, **68**: 429–442.
8. Hutchinson, J.W. and Suo, Z. (1992). Mixed Mode Cracking in Layered Materials, *Advances in Applied Mechanics*, **29**: 63–191.
9. Liechti, K.M. and Liang, Y.M. (1992). The Interfacial Fracture Characteristics of Bimaterial and Sandwich Blister Specimens, *International Journal of Fracture*, **55**, 95–114.
10. Kallas, M.N., Koss, D.A., Hahn, H.T. and Hellman, J.R. (1992). Interfacial Stress State Present in a Thin Slice Fiber Push-out Test, *Journal of Materials Science*, **27**: 3821–3826.
11. Gundel, D.B., Majumdar, B.S. and Miracle, D.B. (1995). Evaluation of the Transverse Response of Fiber-reinforced Composites using a Cross-shaped Sample Geometry, *Scripta Metal*, **3**: 2057–2065.

12. Krawczak, P. and Pabiot, J. (1995). Fracture Mechanics Applied to Glass Fiber/Epoxy Matrix Interface Characterization, *Journal of Composite Materials*, **29**: 2230–2253.
13. Xu, L.R., Huang, Y.Y. and Rosakis, A.J. (2003). Dynamic Crack Deflection and Penetration at Interfaces in Homogeneous Materials: Experimental Studies and Model Predictions, *Journal of Mechanics and Physics of Solids*, **51**: 425–460.
14. Thostenson, E.T., Li, W., Wang, D., Ren, Z. and Chou, T. (2001). Interfacial Characterization of Carbon Nanotube-modified Graphite Fiber Composites, In: *Proceedings of the Sixteenth American Society of Composites Technical Conference*, CRC Press, Boca Raton.
15. Xu, L.R., et al. (2004a). Mechanical Property Characterization of a Polymeric Nanocomposite Reinforced by Graphitic Nanofibers with Reactive Linkers, *Journal of Composite Materials*, **38**: 1563–1582.
16. Aveston, J., Cooper, G.A. and Kelly, A. (1971). Single and Multiple Fracture. The Properties of Fiber Composites, *Conference Proceedings, National Physical Laboratory*, 15–26.
17. Agarwal, V.K. (1978). Axisymmetric Solution of the End-problem for a Semi-infinite Elastic Circular Cylinder and its Application to Joined Dissimilar Cylinders Under Uniform Tension, *International Journal of Engineering Science*, **16**: 985–998.
18. Freund, L.B. (1992). The Axial Force Needed to Slide a Circular Fiber along a Hole in an Elastic Material and Implications for Fiber Pull-out, *European Journal of Mechanics and Solids*, **11**: 1–19.
19. Liang, C. and Hutchinson, J.W. (1993). Mechanics of the Fiber Pushout Test, *Mechanics of Materials*, **14**: 207–221.
20. Povirk, G.L. and Needleman, A. (1993). Finite Element Simulations of Fiber Pull-out, *Journal of Applied Mechanics*, **115**: 286–291.
21. Pochiraju, K.V., Lau, A.C.W. and Wang, A.S.D. (1994). A Local-Global Matching Method for the Single Fiber Pullout Problem with Perfectly Bonded Interface, *Composites Mechanics*, **14**: 84–89.
22. Zhou, L.M., Mai, Y.W. and Ye, L. (1995). Analyses of Fiber Push-out Test based on the Fracture Mechanics Approach, *Composites Engineering*, **5**: 1199–1219.
23. Tsai, K.H. and Kim, K.S. (1996). The Micromechanics of Fiber Pull-out, *Journal of Mechanics and Physics of Solids*, **44**: 1147–1177.
24. Bechel, V.T. and Sottos, N.R. (1998a). Application of Debond Length Measurements to Examine the Mechanics of Fiber Push-out, *Journal of Mechanics and Physics of Solids*, **46**: 1675–1697.
25. Bechel, V.T. and Sottos, N.R. (1998b). Comparison of Calculated and Measured Debond Lengths from Fiber Push-out Test, *Composites Science and Technology*, **58**: 1727–1739.
26. Larson, M.C. and Miles, H.F. (1998). On the Effects of Friction, Roughness and Toughness on Interfacial Sliding in Brittle Composites, *Mechanics of Materials*, **27**: 77–89.
27. Tandon, G.P. and Pagano, N.J. (1998). Micromechanical Analysis of Fiber Push-out and Re-push Test, *Composites Science and Technology*, **58**: 1709–1725.
28. Sridhar, N., Yang, Q.D. and Cox, B.N. (2003). Slip, Stick, and Reverse Slip Characteristics During Dynamic Fiber Pullout, *Journal of the Mechanics and Physics of Solids*, **51**: 1215–1241.
29. Lara-Curzio, E. and Ferber, M.K. (1996). Determination of Interfacial Properties and Stresses in Continuous Fiber-reinforced Ceramic Composites by means of Single-fiber Indentation Tests, In: Bull, J.W. (ed.), *Numerical Analysis and Modelling of Composite Materials*, Blackie Academic and Professional, Glasgow, 642NZ.
30. Greszczuk, L.B. (1969). Theoretical Studies of the Mechanics of the Fiber–matrix Interface in Composites, In: *Interfaces in Composites, ASTM Special Technical Publication, STP-452*, American Society for Testing and Materials, Philadelphia, PA.
31. Curtin, W.A., Eldridge, J.I. and Srinivasan, G.V. (1993). Push-out Tests on a New Silicon Carbide/Reaction-bonded Silicon Carbide Ceramic Matrix Composite, *Journal of American Ceramic Society*, **76**: 2300–2304.
32. Cordes, R.D. and Daniel, I.M. (1995). Determination of Interfacial Properties from Observations of Progressive Fiber Debonding and Pullout, *Composites Engineering*, **5**: 633–648.

33. Pochiraju, K.V., Tandon, G.P. and Pagano, N.J. (2001). Analyses of Single Fiber Pushout Considering Interfacial Friction and Adhesion, *Journal of the Mechanics and Physics of Solids*, **49**: 2307–2338.
34. Pitkethly, M.J., Favre, J.P. and Gaur, U. (1993). A Round-Robin Programme on Interfacial Test Methods, *Composites Science and Technology*, **48**: 205–214.
35. Beckert, W. and Lauke, B. (1997). Critical Discussion of the Single Fibre Pullout Test: Does it Measure Adhesion?, *Composites Science and Technology*, **57**: 1689–1706.
36. Ji, X., Zheng, B.L., Wang, Y.G. and He, P.F. (1997). The Singularity of Stress Field near the Axisymmetric Interface End of Push-in Test Specimen of Composites, *Key Engineering Materials*, **145**: 529–536.
37. Zheng, B.L. and Ji, X. (2002). Stress Singularity Analyses of Interface Ends in Micro-mechanics Tests, *Composites Science and Technology*, **62**: 355–365.
38. Reedy, E.D. and Guesh, T.R. (1993). Comparison of Butt Tensile Strength Data with Interface Corner Stress Intensity Factor Prediction, *International Journal of Solids & Structures*, **30**: 2929–2936.
39. Akisanya, A.R. and Meng, C.S. (2003). Initiation of Fracture at the Interface Corner of Bi-material Joints, *Journal of the Mechanics and Physics of Solids*, **51**: 27–46.
40. Needleman, A. and Rosakis, A.J. (1999). The Effect of Bond Strength and Loading Rate on the Conditions Governing the Attainment of Intersonic Crack Growth along Interfaces, *Journal of Mechanics and Physics of Solids*, **47**: 2411–2449.
41. Tandon, G.P., Kim, R.Y., Warriar, S.G. and Majumdar, B.S. (1999). Influence of Free Edge and Corner Singularities on Interfacial Normal Strength: Application in Model Unidirectional Composites, *Composites, Part B: Engineering*, **30**: 115–134.
42. Kendall, K. (1975). Model Experiments Illustrating Fiber Pullout, *Journal of Materials Science*, **10**: 1011–1014.
43. Atkinson, C., Avila, J., Betz, E. and Smelser, R.E. (1982). The Rod Pull Out Problem, Theory and Experiment, *Journal of Mechanics and Physics of Solids*, **30**: 97–120.
44. Walrath, D.E. and Adams, D.F. (1983). The Iosipescu Shear Test as Applied to Composite Materials, *Experimental Mechanics*, **23**: 105–110.
45. Xu, L.R., Rosakis, A.J. and Samudrala, O. (2002). Measurements of Adhesive Tensile and Shear Strengths with the Aid of Two Optical Techniques, In: *Proceedings of the Society of Experimental Mechanics Annual Conference*.
46. Tippur, H.V., Krishnaswamy, S. and Rosakis, A.J. (1991). A Coherent Gradient Sensor for Crack Tip Deformation Measurements: Analysis and Experimental Results, *International Journal of Fracture*, **48**: 193–204.
47. Williams, M.L. (1952). Stress Singularities Resulting from Various Boundary Conditions in Angular Corners in Extension, *Journal of Applied Mechanics*, **19**: 526–528.
48. Bogy, D.B. (1971). Two Edge-bonded Elastic Wedges of Different Materials and Wedge Angles under Surface Traction, *Journal of Applied Mechanics*, **38**: 377–386.
49. Hein, V.L. and Erdogan, F. (1971). Stress Singularities in a Two-material Wedge, *International Journal of Fracture Mechanics*, **7**: 317–330.
50. Genestedt, J.L. and Hallstrom, S. (1997). Crack Initiation from Homogeneous and Bimaterial Corners, *Journal of Applied Mechanics*, **64**: 811–818.
51. Klingbeil, N.W. and Beuth, J.L. (2000). On the Design of Debond-resistant Bimaterials, Part I: Free-edge Singularity Approach, *Engineering Fracture Mechanics*, **66**, 93–110.
52. Labossiere, P.E.W., Dunn, M.L. and Cunningham, S.J. (2002). Application of Bi-material Interface Corner Failure Mechanics to Silicon/Glass Anodic Bonds, *Journal of Mechanics and Physics of Solids*, **50**: 405–433.
53. Dundurs, J. (1969). Discussion, *ASME Journal of Applied Mechanics*, **36**: 650–652.
54. Mattheck, C. (1998). *Design in Nature: Learning from Trees*, Springer-Verlag, New York.
55. Xu, L.R., Kuai, H. and Sengupta, S. (2004b). Dissimilar Material Joints With and Without Free-edge Stress Singularities, Part-I: A Biologically Inspired Design, *Experimental Mechanics*, **44**: 608–615.

56. Xu, L.R. and Rosakis, A.J. (2002). Impact Failure Characteristics in Sandwich Structures; Part II: Effects of Impact Speed and Interfacial Strength, *International Journal of Solids and Structures*, **39**: 4237–4248.
57. Rice, J.R. (1988). Elastic Fracture Mechanics Concepts for Interfacial Cracks, *Journal of Applied Mechanics*, **55**: 98–103.
58. Kobayashi, A.S. (1987). *Handbook on Experimental Mechanics*, Society for Experimental Mechanics, Inc., Prentice-Hall, New Jersey.